Support information

Origin of Stronger Binding of Ionic Pair (IP) inhibitor to Aβ42 than that of the Equimolar Neutral Counterparts - Synergy Mechanism of IP in Disrupting Aβ42 Protofibril and Inhibiting Aβ42 Aggregation under Two pH Conditions

Wen Xu, Jinfei Mei, Chuanbo Wang Huijuan Yang, Xiaohong Ma, Wenqi Gao, Sajjad Ahmad, Hongqi Ai*

School of Chemistry and Chemical Engineering, University of Jinan, Jinan 250022, PR China

*Corresponding Authors Dr. Hongqi Ai (E-mail: *chm_aihq@ujn.edu.cn*)

Table of Contents

1. Materials and Methods S2

1.1 Model building S2
1.2 Simulation protocol S3
1.3 MM/PBSA binding free energy calculations and energy decompositions S3
1.4 Analytical measures S4

2. Supporting Figures and Tables S6

2.1 Figures S1-S8 ..... S6-S12
2.2 Tables S1-S5 ..... S13-S15

1. Materials and Methods

1.1 Model Building

DAEFRHDSGY(10) EVHHQKLVFF(20) AEDVGSNKGA(30) IIGLMVGGVV(40)IA is the amino acid sequence of Aβ42. Three Aβ42 models were used: Aβ42 monomer (AβM), Aβ42 pentamer (AβP), and LS-type Aβ42 pentamer protofibril (AβF), corresponding to the three development stages of Aβ42 aggregation and evolution (Fig. S2). The full-length AβM and AβF were obtained from RCSB[1] (PDB ID:1IYT[2] and 5OQV,[3] respectively). The AβP structure was obtained from previous laboratory work.[4] 5OQV is a two-fold LS-type $A\beta_{42}$ fibril, from which one-fold LS-type $A\beta_{42}$ protofibril, composed of five Aβ42 chains (pentamer), is taken as present AβF model. The motif of LS-type $A\beta_{42}$ fibril is characterized by three hydrophobic cores, notably Core1: A2, F4, L34 and V36, Core2: L17, F19 and I31, and Core3: A30, I32, M35 and V40 as well as salt bridge between K28 C-terminal A42 of the Aβ42 to stabilize the motif.[3]

To build the above model in an acidic environment, H++ version 4.0 sever[5] was used with pH = 5.5, Salinity = 0.15, and default internal and external dielectric parameters for these models.

The inhibitor structure of the Neu was built by assembling the Head-Neu (4-(1,3-benzothiazol-2-yl)aniline, CID: 234475) and Linker-Tail-Neu section (17-amino-3,6,9,12,15-pentaoxaheptadecan-1-ol, CID: 20554065) from the PubChem[6] website. Then the Linker-Tail section were further refined by Gauss View. Similarly, Pos and Neg were built on the basis of Neu by using Gauss View to add choline and sulfonic acid groups, respectively. The B3LYP/6-31G* technique in Gaussian09 was used to optimize all inhibitor compounds.[7] The Ligand Reader & Modeler[8] module of CHARMM-GUI[9] was employed to produce the force field of the inhibitor molecule.

MGL AutoDock Tools(ADT)[10] was employed for molecular docking during the complex's construction. Water molecules were eliminated during the docking process, polar hydrogen atoms were added, and a computed Gasteiger charge was added. After that, all ligands were docked by integrating nonpolar hydrogen atoms, detecting rotatable bonds. The grid box size of 60 × 60 ×60 Å was produced and assigned to the middle of binding cavity using x, y and z coordinates for the intent searching modality. Other parameters were set to be the default. The Lamarckian genetic algorithm was used to compute the various possible conformation of the ligand molecule and macromolecule. Eventually, 200 poses were adopted finally after docking. In these poses, three structures with the highest conformational probability and the strongest highest binding strength (without result shown) were selected as the optimal complexes to perform the following three parallel simulations. In addition, the complex model was built with a ratio of Aβ42: ligand = 1:2. That is, one Aβ42 monomer corresponds to 2 Neu molecules or 1 IP ((+)BAM1-EG_6 and (-)BAM1-EG_6) due to Aβ42 is a

multiple-target receptor.

When pH is 5.5, six systems of protonated AβM-IP, AβM-Neu, and AβP-IP, AβP-Neu, AβF-IP and AβF-Neu are constructed. In the environment of pH = 7.0, in order to accurately count the effect of IP, three parallel computing systems are constructed for the three systems of IP, namely, AβM-IP1/2/3, AβP-IP1/2/3, AβF-IP1/2/3, respectively. As a result, 15 models for the system with and without Neu were created under neutral conditions. The average results of the last three parallel systems AβY-IPi (I =1,2,3) (Y=M, P, F) are represented by AβY-X_{av}. To dissect the roles of the anionic and cationic species ((+)BAM1-EG_6 and (-)BAM1-EG_6) in IP, two (+)BAM1-EG_6 and (-)BAM1-EG_6) ions are separately docked to AβM to build three parallel AβM-PPi and AβM-NNi models (i=1,2,3) respectively, where PP and NN denote two positive and negative charged BAM1-EG_6. Then six additional models are obtained. The models detail in Table S5.

1.2 Simulation Protocol

All systems were built using the CHARMM-GUI website[9]. In detail, Charmm36 force field[11] and TIP3 water model [12] were used to solve all the systems. Additional amounts of Na^+ were used to neutralize the systems[13]. In all systems, 5000 steepest descent steps are used to minimize energy. The system was then equilibrated for 100ps using the taper (NVT) ensemble and then equilibrated for 100ps to simulate the isobaric isothermal (NPT) ensemble. All systems are run in the NPT set. The LINCS algorithm[14] was used to constrain hydrogen bond lengths in the model. The bond length of water molecule is subject to SETTLE constraint algorithm[15], which also allowed integration time step is 2 fs. Remote electrostatic interactions were calculated using Particle Mesh Ewald[16](PME). Van Der Waals (VDW) interactions were calculated using a 1.2 nm cutoff with a Fourier grid spacing of 0.16 nm. Moreover, the distance between AβY (M, P and F) and the simulated box is 10 Å. The Nose−Hoover temperature coupling[17] was used to control the temperature and the Langevin piston algorithm method[18] was applied to describe the barostat, with coupling times of 0.1 and 1.0ps, respectively. All of the abovementioned dynamic simulations were performed at 310K and 1 bar of pressure by GROMACS[19] version 2020 with periodic conditions applied in all directions. Some simulation details are listed in Table S5.

1.3 MM/PBSA binding free energy calculations and energy decompositions

As the most generally used end point approaches in free energy calculations are Molecular mechanics (MM) and Poisson Boltzmann surface area (PBSA), we employed MM/PBSA[20,21] to compute the binding free energies between small molecules and Aβ42 models.

$$\Delta G = \Delta E_{MM} + \Delta G_{sol} - T\Delta S \quad (1)$$

$$\Delta E_{MM} = \Delta E_{bonded} + \Delta E_{vdw} + \Delta E_{cou} \quad (2)$$

$$\Delta G_{sol} = \Delta G_{polar} + \Delta G_{nonpolar} \quad (3)$$

The ΔG is composed of gas-phase interaction energy (ΔE_{MM}) and solvation free energy (ΔG_{sol}). Among them, the influence of entropy change in binding free energy is not negligible.[22] ΔE_{MM} contains Van Der Waals energy (ΔE_{vdw}), electrostatic interaction energy (ΔE_{cou}) and ΔE_{bonded}; however, ΔE_{bonded} values, such as bond, angle and torsion energies, are often regarded as zero due to identical conformation of the protein–ligand complex in the single trajectory approach. Furthermore, ΔG_{sol} is measured by two energies: the polar energy (ΔG_{polar} also called ΔG_{pb}) estimated by the continuum solvent Poisson–Boltzmann model (PB) and the nonpolar energy ($\Delta G_{nonpolar}$ also known as ΔG_{sa}) estimated by the solvent accessible surface area. As a result, we used equation (4) to determine the binding free energy:

$$\Delta G = \Delta E_{vdw} + \Delta E_{cou} + \Delta G_{pb} + \Delta G_{sa} - T\Delta S \quad (4)$$

To gain crucial residues in the protein–ligand interaction, we calculated the average binding free energy contribution of each residue, and the per-residual MM/PBSA free energy decomposition was also the sum of the Van Der Waals energy (ΔE_{vdw}), electrostatic interaction energy (ΔE_{cou}), polar energy (ΔG_{pb}), nonpolar energy (ΔG_{sa}) and entropy change (TΔS). A more integrated script for binding energy calculation from *https://jerkwin.github.io/2021/03/16/gmx_mmpbsa script updates - shielding effect and the entropy contribution/* was employed as in the script not only the ionic strength is taken into account but also the Debye characteristic length is employed for the ΔE_{cou} calculation to decay the electrostatic interaction exponentially.[23-25]

$$\Delta G_{fit}=0.05402(\Delta E_{cou}+\Delta G_{pb})+0.14852\Delta E_{vdw}+0.05584\Delta G_{np}+0.11351(-T\Delta S_{IE})-4.77148 \quad (5)$$

In order to fit the binding energy more close to the experimental value, a free energy estimator (5) proposed by Huang et al.[26] was finally used to refine these binding free energies (ΔG_{fit}). The free energy estimator was reported to improve correlation coefficient of binding energy from 0.46 (classic MM/PBSA) to 0.72 (ΔG_{fit}), and lower the mean absolute error dramatically from 22.52 to 1.59 kcal/mol for calculating a training set of 84 protein-ligand interactions.

1.4 Analytical measures

We selected the average conformations of compounds produced from stable MD state to investigate the hydrogen bonds and hydrophobic interactions between key residues and inhibitor using LigPlot+[27] in which the default parameters are employed. That is, Hydrogen bond (H-bond) occurs if

D (donor)–A (acceptor) distance is less than 3.5Å and the D–H–A angle larger than 135°. A hydrophobic interaction is defined as the distance in the range of 2.9 Å - 3.9Å between any type atom.

Gromacs[28,29] tools gmx rms, gmx rmsf, gmx do_dssp, gmx hbond, gmx sasa, gmx rdf, gmx mindist were used to calculate root mean square deviation (RMSD), root mean square fluctuation (RMSF), secondary structure, hydrogen bond, solvent accessible surface area, radial distribution function, minimum distance between groups, respectively. Our in-home script was employed to compute the contact number. K_d was obtained by substituting the free energy into the quantitative relationship ($\Delta G = RTlnK_d$) between dissociation constant and binding free energy. Pymol[30] and VMD[31] are utilized for visualization and analysis purposes.

2. Supporting Figures and Tables

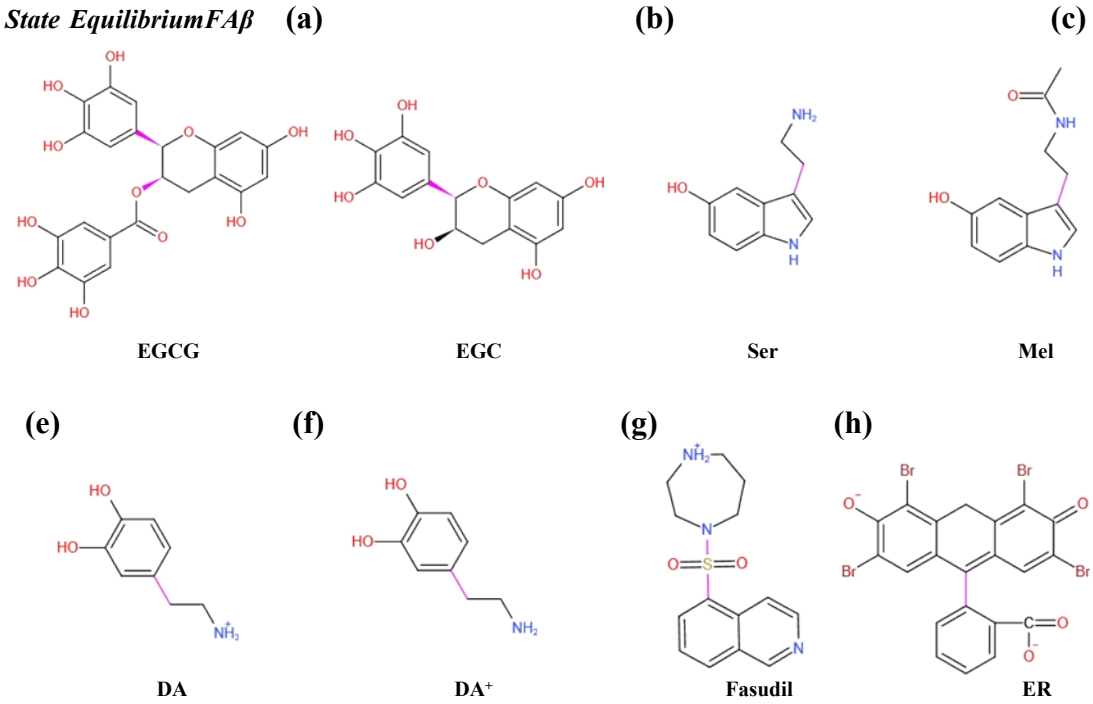

Fig. S1: Structural diagram of neutral and charged small molecules. (a)EGCG[32] (b)EGC[32] (c)Ser[33] (d)Mel[33] (e)DA[34] (f)DA^{+}[34] (g)Fasudil[35] (h)ER[4], where the Linkers are colored in pink.

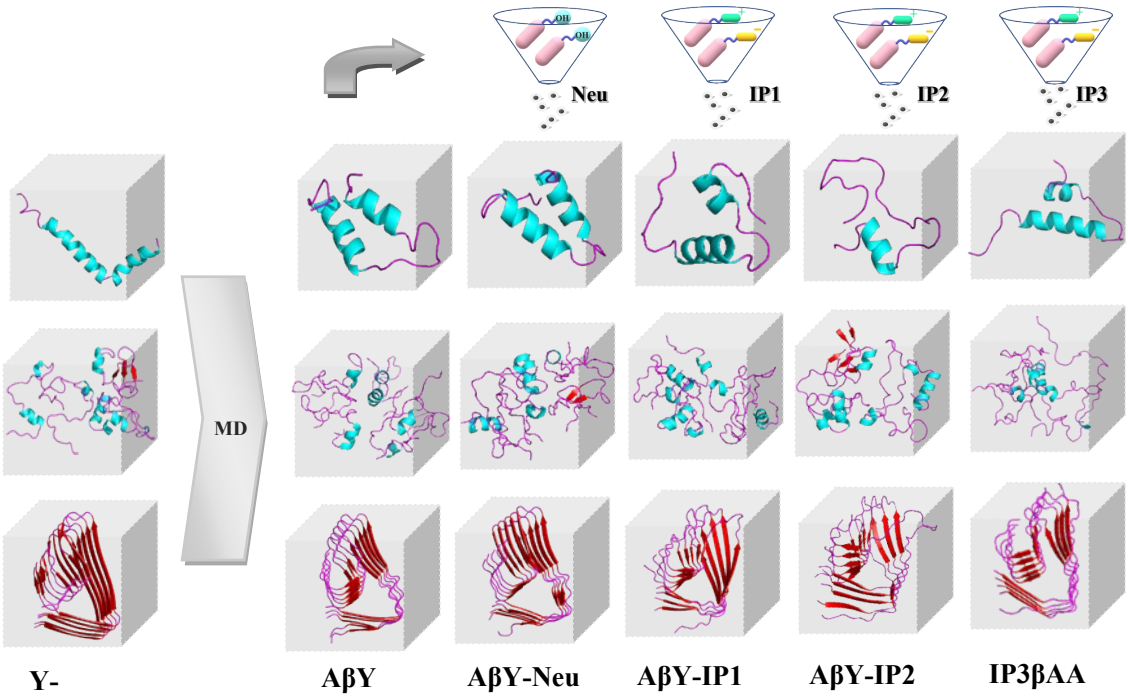

Fig. S2: Three-stage Aβ42 models in the presence or absence of Neu/IP (AβY and AβY-X, Y=M, P and F; X=Neu, IP, NN, and PP) and the changes of AβY configurations. The first column shows the initial states of AβM, AβP, and AβF, which were marked as $A\beta Y_{(i)}$. The second column shows the equilibrated structures of AβM, AβP, and AβF after molecular dynamics simulation. The third column shows the equilibrated structures of AβM, AβP, and AβF after introducing Neu. The third, fourth and fifth columns are the equilibrated AβY structures from three parallel trajectories in the presence of IP.

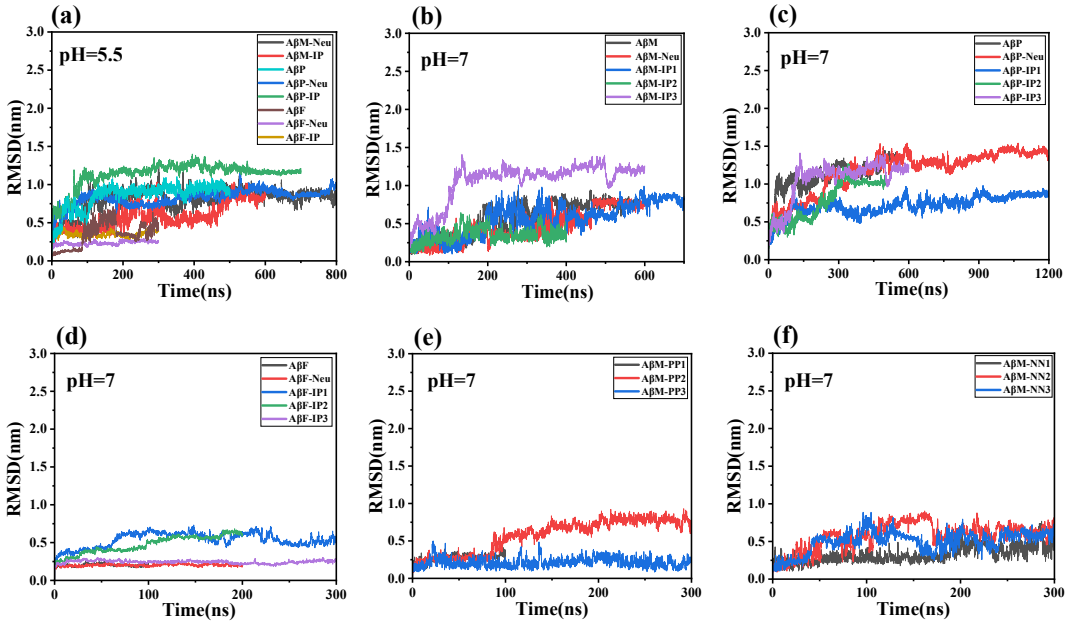

Fig. S3: RMSD diagrams for AβY-Neu/IP at pH = 5.5 (a) and AβY-Neu/IP, AβM-PP_i/NN_i (i=1, 2, and 3) (b-f) at pH = 7.0.

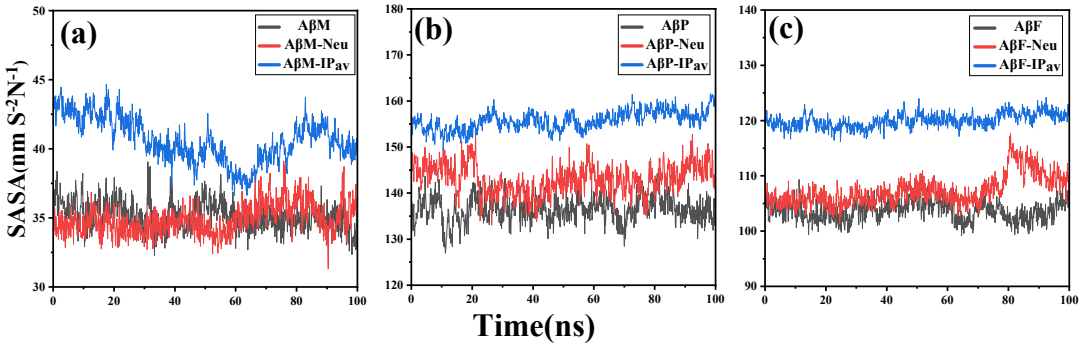

Fig. S4: Evolution of SASA of AβM(a), AβP(b) and AβF(c) during the last 100 ns in the presence of Neu and IP at pH=7.0.

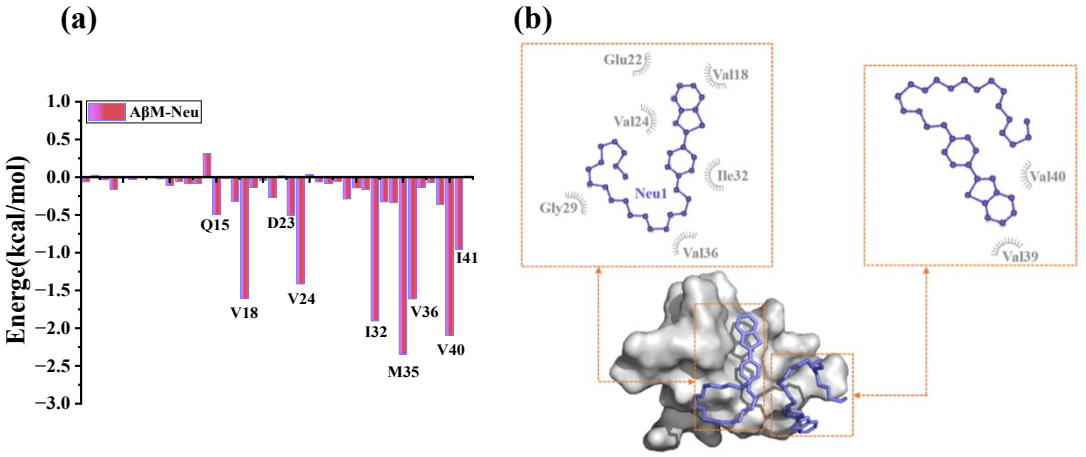

Fig. S5: Residue contributions to the binding energy in AβM-Neu (a) and contact map between AβM and Neu (b). AβM is shown in gray cartoon, and Neu in purple.

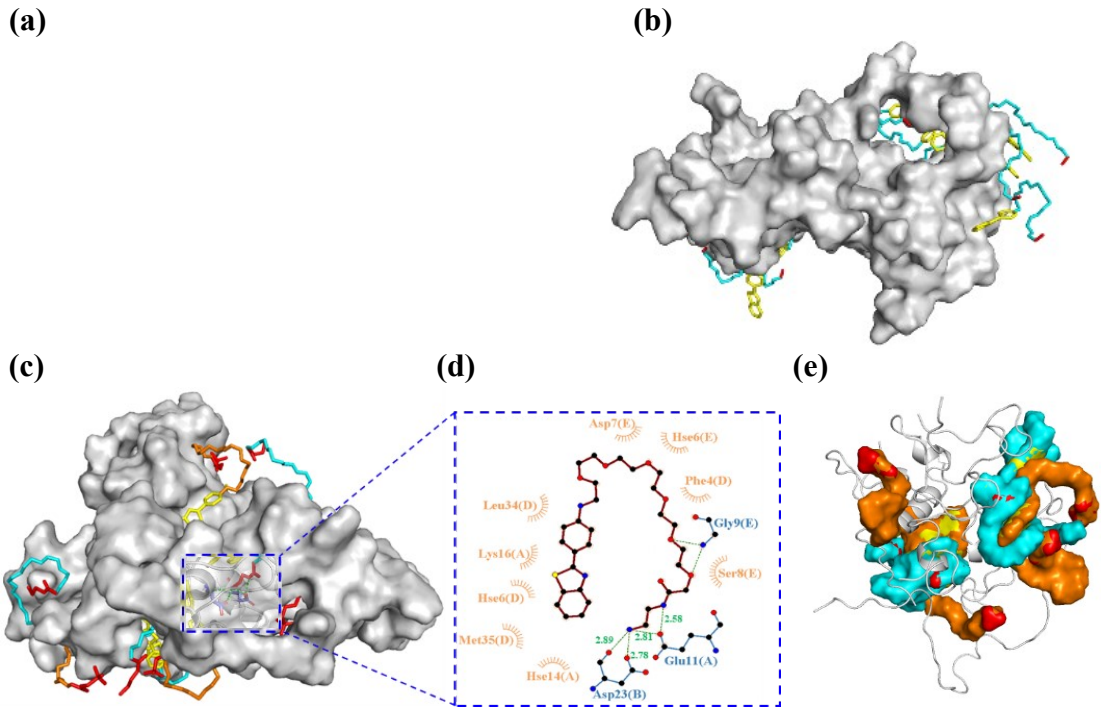

Fig. S6: Snapshots of AβP in the presence of Neu (a, b) and IP (c) at pH = 7.0. An inset from (c) for a Neg embedded in the AβP is displayed in (d). Another exhibition (e) of AβP-IP with AβP section in grey and IP in surface with three different colors to distinguish the three parts of IP. In detail, the head and linker are colored in yellow and cyan, respectively, for IP and Neu, and tails of Pos, Neg, and Neg in orange, red, and red, respectively

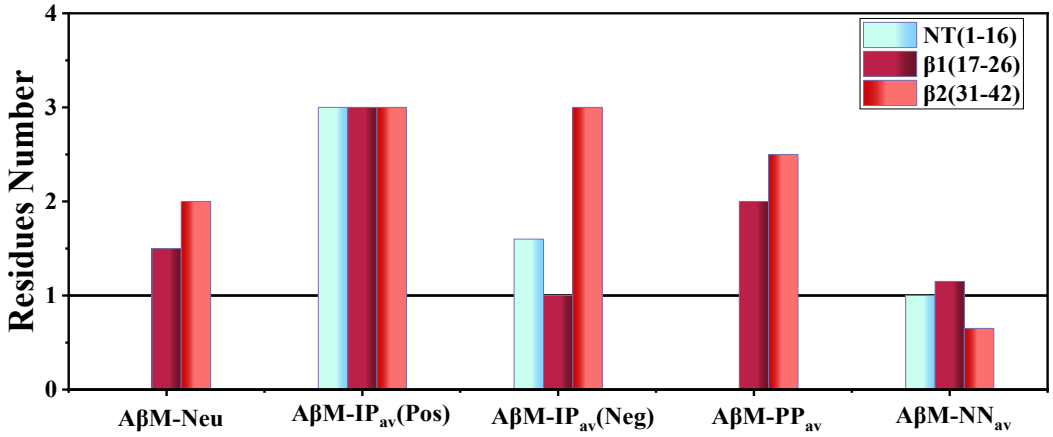

Fig. S7: Number of residues in the NT (1-16), β1 (17-26) and β2 (31-42) regions in AβM interacting to Neu, Pos and Neg, respectively. Subscript av stands for the average of the three parallel systems.

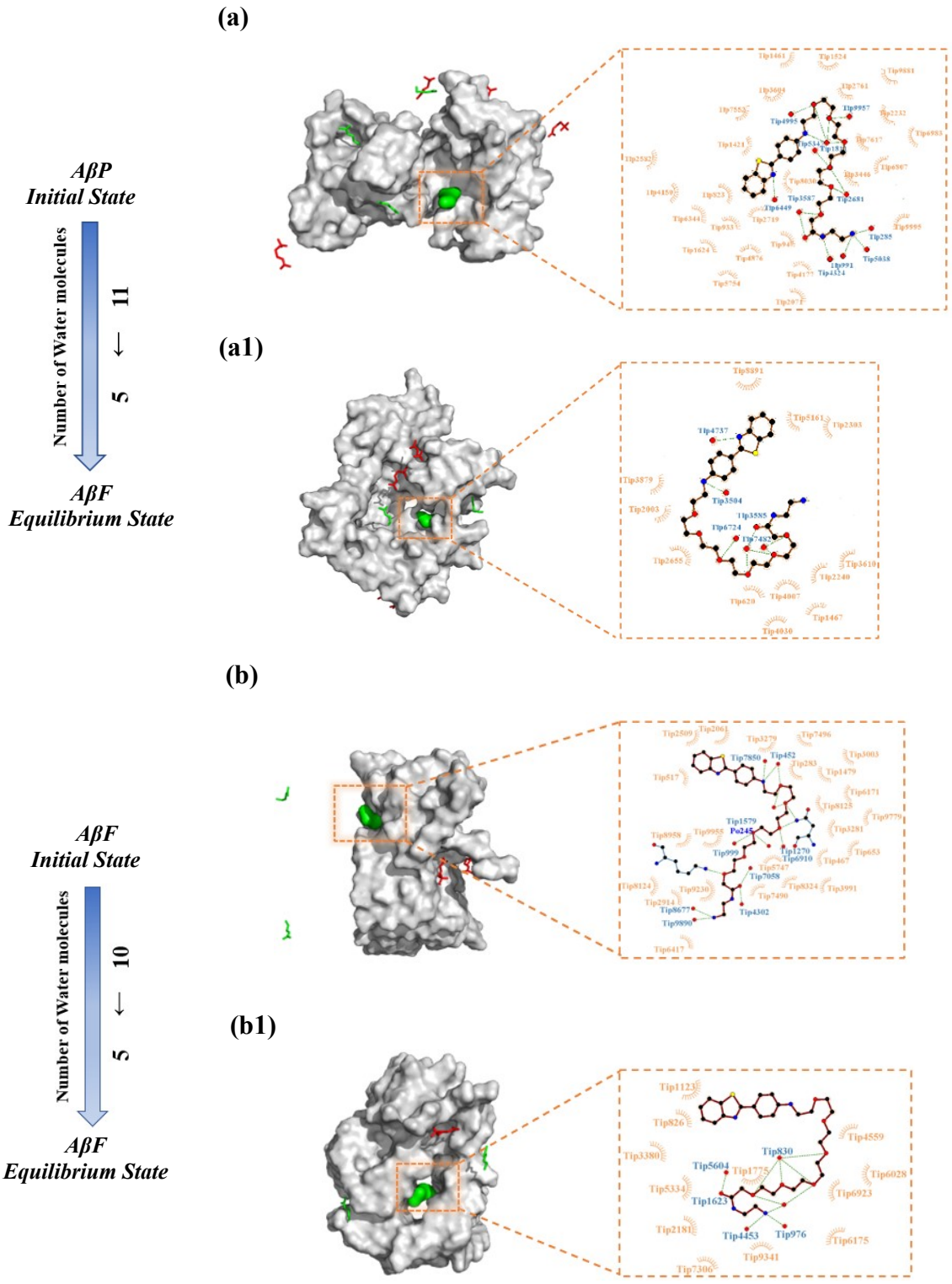
(a)
AβP
Initial State
Number of Water molecules
11
5
AβF
Equilibrium State
(a1)
(b)
AβF
Initial State
Number of Water molecules
10
5
AβF
Equilibrium State
(b1)

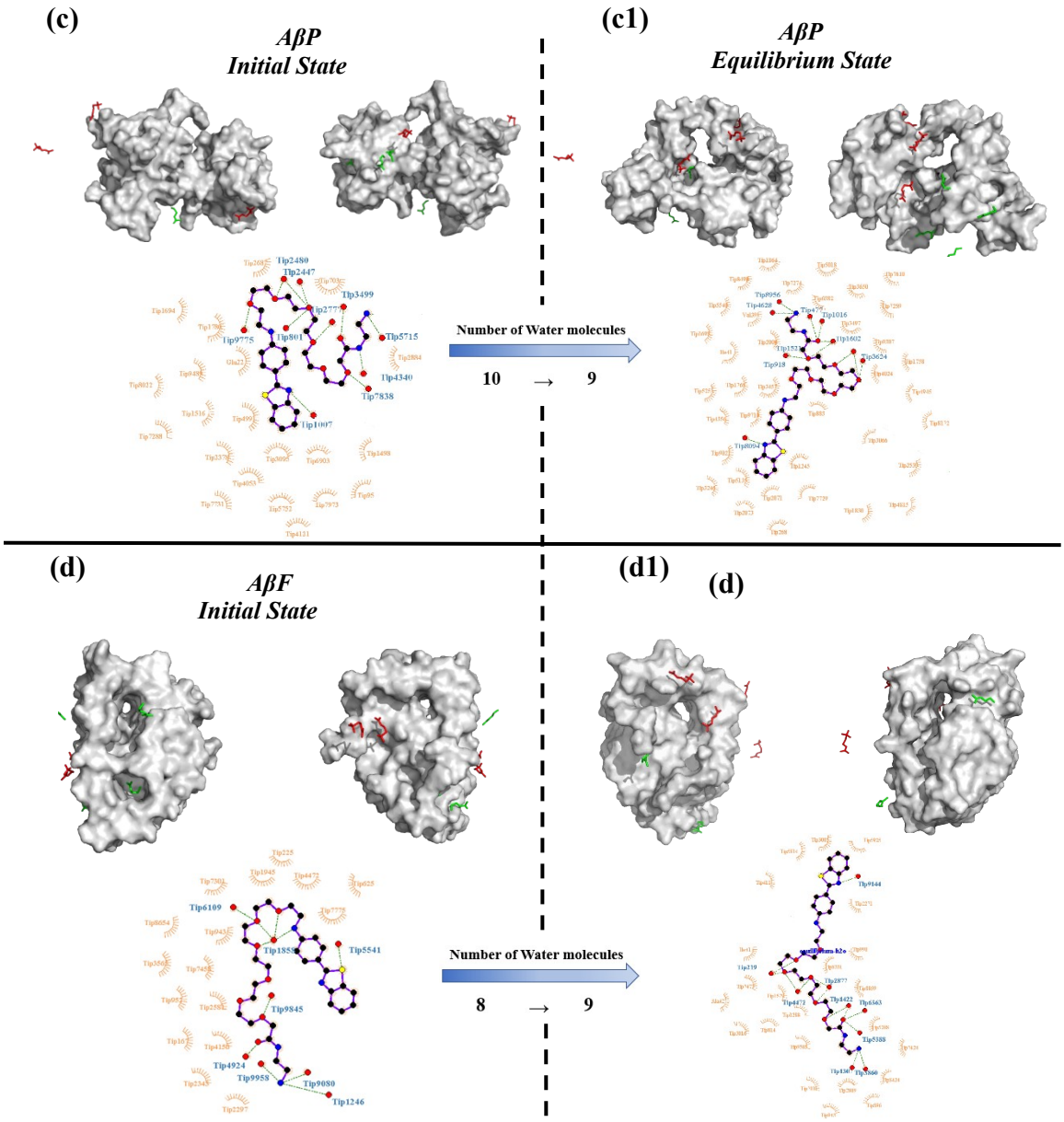

Fig. S8: Number change of water molecules in the first shell (in blue) around a Pos, which is embedded in (a, b) or attached over (c, d) AβP/AβF with its charged tail. (a) and (b) stand for the changes (5-6 water molecules are lost) at pH=7.0, and (c) and (d) at pH=5.5 (±1 water molecule change), respectively. In (c-d), AβP/AβF complexes are shown in both the front and back. The number of water molecules is calculated using LigPlot^{+}[27]. In (c-d), no the positively charged tail of Pos is embedded in the AβP/AβF but attached to the surface, so a hydrated Pos is chosen randomly and displayed.

Table S1 Secondary structure contents (probability of Coil, Sheet, Helix, Turn and Bend) of AβM/AβP/AβF in the presence or absence of Neu/IP/PP/NN.

System	Coil	Sheet	Helix	Turn	Bend
AβM	0.23	0.03	0.56	0.07	0.10
AβM-Neu	0.30	0.00	0.52	0.14	0.04
AβM-IP$_{av}$	0.39±0.07	0.00±0.00	0.37±0.14	0.1±0.03	0.13±0.05
AβM-PP$_{av}$	0.19±0.01	0.00±0.00	0.57±0.02	0.10±0.04	0.12±0.02
AβM-NN$_{av}$	0.23±0.01	0.02±0.01	0.53±0.02	0.09±0.01	0.12±0.01
AβP	0.42	0.06	0.22	0.12	0.18
AβP-Neu	0.41	0.10	0.18	0.14	0.16
AβP-IP$_{av}$	0.37±0.03	0.10±0.03	0.22±0.03	0.13±0.01	0.17±0.02
AβF	0.39	0.46	0.02	0.00	0.13
AβF-Neu	0.22	0.66	0.02	0.00	0.11
AβF-IP$_{av}$	0.31±0.02	0.54±0.01	0.01±0.01	0.01±0.00	0.12±0.01

Table S2 At pH 7.0, the solvent accessible surface area (unit: nMS^{-2}N^{-1}) of AβY in the presence or absence of Neu/IP.

System	AβM	AβM-Neu	AβM-IP$_{av}$	AβP	AβP-Neu	AβP-IP$_{av}$	AβF	AβF-Neu	AβF-IP$_{av}$
SASA	42	36	43	135	141	157	106	111	123

Table S3: Number of contact between hydrophobic residues in NT (1-16), β1 (17-26) and β2 region (31-42) of AβP and Heads of Neu/ Pos/ Neg. AβP-IP$_{av}$ results was obtained by averaging the values of AβP-IP1/2/ 2/3.

System	Head	NT(1-16)	β1(17-26)	β2(31-42)
AβP-IP1	5Pos	4	4	11
	5Neg	5	4	12
AβP-IP2	5Pos	8	4	7
	5Neg	4	4	6
AβP-IP3	5Pos	10	7	8
	5Neg	6	5	8
AβP-IP$_{av}$	5Pos	7.3	5.0	8.6
	5Neg	5.0	4.3	8.6
AβP-Neu	5Neu	3.5	1.5	5.5

Table S4: Hydrogen bonds (HB) and salt bridges (SB) generated between AβP and IP/Neu with its tail. SB-N and HB-N stand for the numbers of SB and HB, respectively. The residues in blue indicate both HB and SB are generated on it synchronously. (A) to (E) in parentheses denote the serial number of five chains in AβP

System	Tail	SB-N	SB residues	HB-N	HB residues
AβP-IP1	5Pos	3.0	D7(C), D23(A), E11(B)	6.0	2D7(C), 2D23(A), E22(A), Y10(C)
	5Neg	1.0	R5(A)	6.0	S26(A),V40(A),Y10(C), R5(A), F4(A), E20(C)
AβP-IP2	5Pos	3.0	D7(C), D23(C), E22(A)	4.0	D7(C), D23(C), S8(C), H6(C)
	5Neg	1.0	K16(A)	2.0	H14(C), S26(C)
AβP-IP3	5Pos	4.0	D23(A), D23(B), E11(A), E11(C)	4.0	D23(A), D23(B), E11(A), K16(C)
	5Neg	0	———	3.0	H13(D), Y10(D), G38(D)
AβP-IP$_{av}$	5Pos	3.3	D(60%), E(40%)	4.7	D(57%), E(14%),Y, S, H, K (7%)
	5Neg	0.7	R, K(50%)	3.7	H, Y, S(18%) V, E, R, F, G (9%)
AβP-Neu	5Neu	0	———	2.0	M(50%), G(50%)

Table S5: Binding free energies (kcal/mol) between AβM and Neu/IP/PP/NN

Complex	ΔE_{vdw}	ΔE_{cou}	ΔG_{pb}	ΔG_{sa}	$-T\Delta S$	ΔG	ΔG_{fit}	K_d(nM)
AβM-Neu	-7.4	-2.0	4.7	-1.1	0.2	-5.5	-5.8	$5.5*10^4$
AβM-IP$_{av}$	-15.0	-11.7	10.5	-1.3	0.4	-17.1	-7.1	$6.16*10^3$
AβM-PP$_{av}$	-31.5	-36.3	53.7	-6.9	19.3	-1.6	-6.7	$1.21*10^4$
AβM-NN$_{av}$	-25.1	-3.3	25.5	-5.7	12.9	4.3	-6.1	$3.34*10^4$

Table S6: Simulation details of 29 systems.

pH	Simulation system	Box size(nM^3)	Simulation time(ns)	Total number of atoms
5.5	**AβM-Neu**	6.62x6.62x6.62	800	29380
5.5	**AβM-IP**	6.63x6.63x6.63	600	29403
5.5	**AβP**	8.35x8.35x8.35	500	57205
5.5	**AβP-Neu**	8.36x8.36x8.36	800	59389
5.5	**AβF**	6.99x6.99x6.99	300	34829
5.5	**AβP-IP**	8.36x8.36x8.36	700	59414
5.5	**AβF-Neu**	7.39x7.39x7.39	300	41121
5.5	**AβF-IP**	7.39x7.39x7.39	300	41121
7	**AβM**	6.63x6.63x6.63	600	29397
7	**AβM-Neu**	6.63x6.63x6.63	600	29335
7	**AβM-IP1**	5.84x5.84x5.84	700	20052
7	**AβM-IP2**	5.96x5.96x5.96	400	21374
7	**AβM-IP3**	6.52x6.52x6.52	600	28004
7	**AβM-PP1**	6.54x6.54x6.54	100	28004
7	**AβM-PP2**	6.53x6.53x6.53	300	28080
7	**AβM-PP3**	6.52x6.52x6.52	300	28083
7	**AβM-NN1**	6.62x6.62x6.62	300	29291
7	**AβM-NN2**	6.62x6.62x6.62	300	29335
7	**AβM-NN3**	6.63x6.63x6.63	300	29369
7	**AβP**	8.25x8.25x8.25	600	59338
7	**AβP-Neu**	8.38x8.38x8.38	1200	59338
7	**AβP-IP1**	8.37x8.37x8.37	1200	59213
7	**AβP-IP2**	8.38x8.38x8.38	500	59312
7	**AβP-IP3**	8.36x8.36x8.36	600	59225
7	**AβF**	7.27x7.27x7.27	100	39188
7	**AβF-Neu**	7.39x7.38x7.39	200	41022
7	**AβF-IP1**	7.40x7.40x7.40	300	40972
7	**AβF-IP2**	7.30x7.30x7.30	200	39363
7	**AβF-IP3**	7.39x7.38x7.39	300	41113

References

1. H. M. Berman , J. Westbrook , Z. Feng , G. Gilliland , T. N. Bhat , H. Weissig , I. N. Shindyalov and P. E. Bourne, *Nucleic. Acids. Res*, 2000, **28**, 235-242.
2. O. Crescenzi , S. Tomaselli , R. Guerrini , S. Salvadori , A. M. D'Ursi , P. A. Temussi and D. Picone, *Eur J Biochem*, 2002, **269**, 5642-5648.
3. L. Gremer , D. Schölzel , C. Schenk , E. Reinartz , J. Labahn , R. B. G. Ravelli , M. Tusche , C. Lopez-Iglesias , W. Hoyer , H. Heise , D. Willbold and G. F. Schröder, *Science (New York, N.Y.)*, 2017, **358**, 116-119.
4. J. Mei , H. Yang , B. Sun , C. Liu and H. Ai, *ACS Chem Neurosci*, 2021, **12**, 1197-1209.
5. B. A. Alexey Onufriev.Ramu Anandakrishnan, John Gordon,Jonathan Myers,Timothy Folta,Valia Shoja,Lenwood S. Heath,Cliff Shaffer,Godmar Back,Derek Rountree,Jory Zmuda Ruscio,Yuri Pevzner, *H++*, 2004.
6. S. Kim , P. A. Thiessen , E. E. Bolton , J. Chen , G. Fu , A. Gindulyte , L. Han , J. He , S. He , B. A. Shoemaker , J. Wang , B. Yu , J. Zhang and S. H. Bryant, *Nucleic. Acids. Res*, 2016, **44**, D1202-1213.
7. M. J. Frisch, Trucks, G. W., Schlegel, H. B., Scuseria, G. E., Robb, M. A., Cheeseman, J. R., Scalmani, G., Barone, V., Mennucci, B., Petersson, G. A., Nakatsuji, H., Caricato, M., Li, X., Hratchian, H. P., Izmaylov, A. F., Bloino, J., Zheng, G., Sonnenberg, J. L., Hada, M., Ehara, M., Toyota, K., Fukuda, R., Hasegawa, J., Ishida, M., Nakajima, T., Honda, Y., Kitao, O., Nakai, H., Vreven, T., Montgomery, J. A., Jr., Peralta, J. E., Ogliaro, F., Bearpark, M. J., Heyd, J., Brothers, E. N., Kudin, K. N., Staroverov, V. N., Kobayashi, R., Normand, J., Raghavachari, K., Rendell, A. P., Burant, J. C., Iyengar, S. S., Tomasi, J., Cossi, M., Rega, N., Millam, N. J., Klene, M., Knox, J. E., Cross, J. B., Bakken, V., Adamo, C., Jaramillo, J., Gomperts, R., Stratmann, R. E., Yazyev, O., Austin, A. J., Cammi, R., Pomelli, C., Ochterski, J. W., Martin, R. L., Morokuma, K., Zakrzewski, V. G., Voth, G. A., Salvador, P., Dannenberg, J. J., Dapprich, S., Daniels, A. D., Farkas, Ö, Foresman, J. B., Ortiz, J. V., Cioslowski, J., and Fox , D. J. , *Gaussian09*, 2009.
8. S. Kim , J. Lee , S. Jo , C. L. Brooks, 3rd , H. S. Lee and W. Im, *J Comput Chem*, 2017, **38**, 1879-1886.
9. S. Jo , T. Kim , V. G. Iyer and W. Im, *J Comput Chem*, 2008, **29**, 1859-1865.
10. S. Forli , R. Huey , M. E. Pique , M. F. Sanner , D. S. Goodsell and A. J. Olson, *Nat Protoc*, 2016, **11**, 905-919.
11. J. Lee , X. Cheng , J. M. Swails , M. S. Yeom , P. K. Eastman , J. A. Lemkul , S. Wei , J. Buckner , J. C. Jeong , Y. Qi , S. Jo , V. S. Pande , D. A. Case , C. L. Brooks, 3rd , A. D. MacKerell, Jr. , J. B. Klauda and W. Im, *J Chem Theory Comput*, 2016, **12**, 405-413.
12. W. L. Jorgensen , J. Chandrasekhar , J. D. Madura , R. W. Impey and M. L. Klein, *J Chem Phys*, 1983, **79**, 926-935.
13. S. K. Mudedla , N. A. Murugan and H. Agren, *ACS Chem Neurosci*, 2019, **10**, 1347-1354.

14. B. B. Hess, Henk; Berendsen, Herman J. C.; Fraaije, Johannes G. E. M., *J Comput Chem*, 1997, **18**, 1463-1472.
15. Y. Qiu , A. Mekkat , H. Yu , S. Yigit , S. Hamaia , R. W. Farndale , D. L. Kaplan , Y. S. Lin and B. Brodsky, *J Struct Biol*, 2018, **203**, 255-262.
16. T. Darden , D. York and L. Pedersen, *J Comput Chem*, 1993, **98**, 10089-10092.
17. W. G. Hoover, *Phys Rev A*, 1985, **31**, 1695-1697.
18. S. E. Feller, Zhang, Y., Pastor, R. W. & Brooks, B. R, *J Chem Phys*, 1995, **103**, 4613–4621.
19. G. M. Morris , R. Huey , W. Lindstrom , M. F. Sanner , R. K. Belew , D. S. Goodsell and A. J. Olson, *J Comput Chem*, 2009, **30**, 2785-2791.
20. N. A. Baker , D. Sept , S. Joseph , M. J. Holst and J. A. McCammon, *Proc Natl Acad Sci U S A*, 2001, **98**, 10037-10041.
21. R. Kumari , R. Kumar and A. Lynn, *J Chem Inf Model*, 2014, **54**, 1951-1962.
22. Y. J. Sheng , Y. W. Yin , Y. Q. Ma and H. M. Ding, *J Chem Inf Model*, 2021, **61**, 2454-2462.
23. S. Genheden and U. Ryde, *Expert Opin Drug Discov*, 2015, **10**, 449-461.
24. K. Colwill , Y. Galipeau , M. Stuible , C. Gervais , C. Arnold , B. Rathod , K. T. Abe , J. H. Wang , A. Pasculescu , M. Maltseva , L. Rocheleau , M. Pelchat , M. Fazel-Zarandi , M. Iskilova , M. Barrios-Rodiles , L. Bennett , K. Yau , F. Cholette , C. Mesa , A. X. Li , A. Paterson , M. A. Hladunewich , P. J. Goodwin , J. L. Wrana , S. J. Drews , S. Mubareka , A. J. McGeer , J. Kim , M. A. Langlois , A. C. Gingras and Y. Durocher, *Clin Transl Immunol*, 2022, **11**, e1380.
25. H. Sun , Y. Li , S. Tian , L. Xu and T. Hou, *Phys Chem Chem Phys*, 2014, **16**, 16719-16729.
26. K. Huang , S. Luo , Y. Cong , S. Zhong , J. Z. H. Zhang and L. Duan, *Nanoscale*, 2020, **12**, 10737-10750.
27. R. Laskowski, *LigPlot*$^{+}$, 2009.
28. W. Kabsch and C. Sander, *Biopolymers*, 1983, **22**, 2577-2637.
29. X. Daura, Gademann, K., Jaun, B., Seebach, D., van Gunsteren, W. F., and Mark, A. E., *Angew Chem, Int. Ed.*, 1999, **38**, 236– 240.
30. W. L. DeLano, *CCP4 Newsletter on Protein Crystallography*, 2002, **40**, 82-92.
31. W. D. Humphrey, Andrew; Schulten, Klaus, *J Mol Graph Model*, 1996, **14**, 33-38.
32. C. Zhan , Y. Chen , Y. Tang and G. Wei, *ACS Chem Neurosci*, 2020, **11**, 1841-1851.
33. Y. Gong , C. Zhan , Y. Zou , Z. Qian , G. Wei and Q. Zhang, *ACS Chem Neurosci*, 2021, **12**, 799-809.
34. Y. Chen , X. Li , C. Zhan , Z. Lao , F. Li , X. Dong and G. Wei, *ACS Chem Neurosci*, 2021, **12**, 4007-4019.
35. P. Robustelli , A. Ibanez-de-Opakua , C. Campbell-Bezat , F. Giordanetto , S. Becker , M. Zweckstetter , A. C. Pan and D. E. Shaw, *J Am Chem Soc*, 2022, **144**, 2501-2510.